

# Memory Loss in Holographic Non-equilibrium Heating

D.S.Ageev and I.Ya.Aref'eva

*Steklov Mathematical Institute, Russian Academy of Science*

We consider the time evolution of entanglement entropy after a global quench in a strongly coupled holographic two-dimensional system with initial temperature  $T_i$ . Subsequent equilibration increases the temperature up to a final temperature  $T_f$ . We describe this process holographically by an injection of a thin shell of matter in the black hole background with temperature  $T_i$ .

In the limit of large regions of entanglement, the evolution of entanglement entropy at large times becomes a function of one variable  $\Delta S(\tau, \ell) \sim \mathfrak{M}(\tau - \ell)$ . This is a so called memory loss regime well known for the holographic thermalization from zero temperature. We evaluate specific characteristics of this regime in nonequilibrium heating and find that the behaviour of the function  $\mathfrak{M}(t - \ell)$  during post-local-equilibration and saturation times has similar forms as for thermalization from zero temperature, but the scaling coefficients depend on the temperature difference  $T_f - T_i$ .

## CONTENTS

I. Introduction	1
II. Setup	2
A. Length of the ETEBA geodesics describing thermalization	2
B. Length of the ETEBA geodesics describing non-equilibrium heating	2
C. Different regimes in equilibration	3
D. Scaling characteristics of thermalization regimes	4
III. Critical curve	4
IV. Memory loss regime in non-equilibrium heating	5
A. Saturation. Expansion near $\pi/2$	6
B. Post-local-equilibration linear growth. Expansion near $\vartheta_\kappa$	7
C. Late-time memory loss regime. Interpolation between $\phi = \vartheta_\kappa$ and $\pi/2$	8
V. Numerical results	8
VI. Conclusions and discussions	8
Acknowledgements	10
References	10

## I. INTRODUCTION

It is universally recognized that one of the most challenging questions in traditional methods of quantum field theories is the description of thermalization process. The AdS/CFT correspondence [1–3] proposes a powerful tool for a description of thermalization process in general class of strong coupling quantum theories. In the holographic duality the temperature in the quantum field theory is related with the black hole (or black brane) temperature

in the dual background [4]–[6]. The description of the thermalization of conformal field theory after a global quench is well known [7, 8] and in the dual language the thermalization is described by a black hole formation, see [9, 10] and references therein. Also see [11–13] for different applications of the AdS/CFT duality. The simplest description of this process is provided by the Vaidya deformation of a given background, see [14]–[36] and references therein.

However not all interesting non-equilibrium processes in strong correlated systems start from zero temperature. In [35] the global quench starting from the thermal initial state has been considered for some particular simple models. Many interesting and noteworthy phenomena start from non-zero temperatures, in particular, all phenomena related with biological systems. So it is natural to try to study these phenomena using the gravity dual description. In particular, such approach has been used in the holographic description of the photosynthesis [36].

In some sense the non-equilibrium heating process as compared to the thermalization is simpler to study, but holographically the situation is just opposite. It is natural to expect that non-equilibrium heating inherits typical regimes taking place during thermalization. The regimes in thermalization processes have been studied in details in the papers by H.Liu and S.Suh [20, 21], see also [37–39], and they are – regimes of pre-local-equilibration quadratic growth, post-local-equilibration linear growth, a late-time regime in which the evolution does not carry any memory of the size and shape of the entangled region, and the saturation regime. In this paper we show that this is really true for 1+1 dimensional systems, whose dual admits the explicit formula [24], but curiously calculations of scaling coefficients are more involved, as compared to those of the thermalization.

The paper is organized as follows. In Section II we remind the dual geometry of the thermalization and non-equilibrium heating processes and present the explicit formulae for the entanglement entropy evolution after the global quench in initially thermal system. We also list the specific regimes during these processes and remind the

previous results about behavior of the entanglement entropy during thermalization. Section III is devoted to the study of detailed relations between geometrical characteristics of the entanglement minimal surface (geodesic) in the bulk and physical parameters on the boundary, that are the size  $\ell$  of the entangled area and thermalization time  $\tau$  of this area. In Section IV we calculate the scaling characteristics of the memory loss regime in the process of the global quench in thermal system with temperature  $T_i \neq 0$  and especially their dependences on the difference between final and initial temperatures. In the final Section VI we conclude and we discuss some possible generalizations.

## II. SETUP

### A. Length of the ETEBA geodesics describing thermalization

According to the AdS/CFT prescription, the Vaidya-AdS geometry describes thermalization

$$ds^2 = \frac{R^2}{z^2} (-f(v, z)dv^2 - 2dv dz + d\vec{x}^2), \quad (2.1)$$

with  $f(v, z) = 1 - \theta(v)g(z)$ . Where the function  $h(z) \equiv 1 - g(z)$  describes different final equilibrium states. The entanglement entropy  $S$  of the interval with length  $\ell$  in the holographic model [40, 41] of thermalization is given by the length of the ETEBA geodesics. The ETEBA (this terminology has been introduced in [25]) geodesics are spacelike geodesics with both endpoints anchored on the boundary, at the same time  $\tau$  and located on the distance  $\ell$ . For the case of  $g(z) = z^2/z_h^2$  this length is described by the following formula [27]

$$S(\ell, \tau) = \log \left( \frac{z_h}{\ell s} \sinh \frac{\tau}{z_h} \right), \quad (2.2)$$

where  $s$  is a geometric parameter that together with additional parameter  $\rho$  specify the top of the ETEBA geodesics  $z_*$  (its furthest from the boundary point in the bulk) and its intersection point  $z_c$  with the null shell,

$$s = \frac{z_c}{z_*}, \quad \rho = \frac{z_h}{z_c}, \quad (2.3)$$

here  $s$  and  $\rho$  are implicitly related with the time  $\tau$  and length  $\ell$  via the set of two equations

$$\frac{\tau}{z_h} = \text{arccoth} \left( \frac{c + 2\rho^2 + 2c\rho^2}{2c\rho + 2\rho} \right), \quad (2.4)$$

$$\ell = \ell_+ + \ell_-, \quad (2.5)$$

$$\frac{\ell_-}{z_h} = \frac{c}{\rho s}, \quad \frac{\ell_+}{z_h} = \log \frac{2(1+c)\rho^2 + 2s\rho - c}{2(1+c)\rho^2 - 2s\rho - c}, \quad (2.6)$$

where  $c = \sqrt{1-s^2}$ ,  $0 \leq s \leq 1$  and  $0 < \rho$ . These three equations (2.2), (2.4) and (2.5) totally describe the evolution of the entanglement entropy during thermalization.

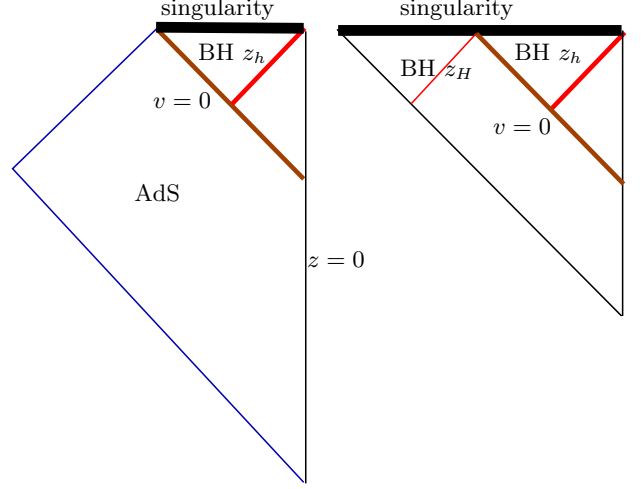


FIG. 1. The plot of the Penrose diagrams for the Vaidya metrics (2.1) and (2.7).

### B. Length of the ETEBA geodesics describing non-equilibrium heating

In this paper we consider black hole collapsing from the initial state defined by the horizon position  $z_H$  to the final state with horizon  $z_h$  as a dual background. The BH-Vaidya metric is given by

$$ds^2 = \frac{R^2}{z^2} (-f(v, z)dv^2 - 2dv dz + d\vec{x}^2), \quad (2.7)$$

where

$$f(z, v) = \theta(v)f_h(z) + \theta(-v)f_H(z), \quad (2.8)$$

and the functions  $f_H$  and  $f_h$  are defined as

$$f_H = 1 - \left( \frac{z}{z_H} \right)^2, \quad f_h = 1 - \left( \frac{z}{z_h} \right)^2, \quad z_h < z_H. \quad (2.9)$$

The time is related with variable  $v$  as

$$v < 0 \quad t = v + z_H \text{arctanh} \frac{z}{z_H}, \quad (2.10)$$

$$v > 0 \quad t = v + z_h \text{arctanh} \frac{z}{z_h}. \quad (2.11)$$

The initial and final temperatures, energy and entropy are

$$T_i = \frac{1}{2\pi z_H}, \quad T_f = \frac{1}{2\pi z_h}, \quad (2.12)$$

$$\mathcal{E}_i = \frac{R}{8\pi G_N} \frac{1}{z_H^2}, \quad \mathcal{E}_f = \frac{R}{8\pi G_N} \frac{1}{z_h^2}, \quad (2.13)$$

$$s_i = \frac{R}{z_H} \frac{1}{4G_N}, \quad s_f = \frac{R}{z_h} \frac{1}{4G_N}, \quad (2.14)$$

where  $G_N$  is Newton's constant in the bulk and  $R$  is a typical scale in the bulk. In this paper we set  $8\pi G_N/R =$

1. This metric describes the shell located at  $v = 0$  and usually  $z_H > z_h$ . Note, that the case  $z_H < z_h$  corresponds to a model of cooling [18] and this model violates NEC condition [20].

We have solved this model explicitly [24] and we have obtained the following expression for the entanglement entropy

$$S = \log \left( \frac{z_h}{\ell \mathfrak{S}_\kappa(\rho, s)} \sinh \frac{\tau}{z_h} \right), \quad (2.15)$$

where  $\mathfrak{S}_\kappa$  is given by

$$\mathfrak{S}_\kappa(\rho, s) = \frac{c\rho + \Delta}{\Delta} \cdot \sqrt{\frac{\Delta^2 - c^2\rho^2}{\rho(c^2\rho + 2c\Delta + \rho) - \kappa^2}}. \quad (2.16)$$

$$\ell_+ = \frac{z_h}{2} \log \left( \frac{c^2\gamma^4 - 4\Delta (cs(\kappa^2 - 2\rho^2 + 1) + \Delta + \Delta(\rho^2 - 2)s^2)}{c^2\gamma^4 - 4\Delta^2(\rho s - 1)^2} \right), \quad \ell_- = \frac{z_h}{2\kappa} \log \left( \frac{(c\kappa + \Delta s)^2}{\rho^2 s^2 - \kappa^2} \right), \quad (2.19)$$

where in addition to (2.3) we introduce

$$\kappa = \frac{z_h}{z_H} < 1. \quad (2.20)$$

In (2.24) we also use the notations

$$c = \sqrt{1 - s^2}, \quad (2.21)$$

$$\gamma = 1 - \kappa^2, \quad (2.22)$$

$$\Delta = \sqrt{\rho^2 - \kappa^2}. \quad (2.23)$$

The bulk variables define relative position of the geodesic top  $z_*$  and the point where geodesic crosses the null shell  $z_c$ . Now there are restrictions  $z_* < z_H$  and  $z_c < z_H$ , but there are still 3 types of ETEBA geodesics.

For  $\tau < 0$  our ETEBA geodesic (first type) lies entirely in the BTZ bulk with temperature  $T_i$ . The entanglement entropy is independent on  $\tau$  and is equal (after the minimal renormalization) to

$$S_i = \log \left( \frac{z_H}{\ell} \sinh \frac{\ell}{z_H} \right). \quad (2.24)$$

The top of the corresponding ETEBA geodesic  $z_* < z_H$  and  $z_* \rightarrow z_H$  when  $\ell$  increases in the correspondence with [37]. Let us fix  $\ell$  and start to increase the time.

At very small  $\tau > 0$ , the ETEBA geodesic starts intersecting the null shell and for  $\tau \ll z_h$  the point of intersection is close to the boundary,  $z_c \ll z_h$ . This is the second type of the ETEBA geodesics. When  $\tau$  is of order  $z_h$  the ETEBA geodesic (third type) intersects the shell behind the horizon, i.e.  $z_c > z_h$ . At some time  $\tau = \tau_s$  the ETEBA geodesic lies entirely in the black hole (with the temperature  $T_f$ ) region.

The role of the second horizon located at  $z = z_H$  is that it pulls out of the ETEBA geodesic with the top  $z_* > z_h$  to the first horizon, and this effect is stronger as the difference of two temperatures decrease, i.e.  $\kappa \rightarrow 1$ .

The entanglement entropy (2.16) has been obtained as a length of the ETEBA geodesic with minimal divergence subtraction. Both endpoints of these geodesic are anchored on the boundary points at the same time  $\tau$  located on the distance  $\ell$ . The relations between the boundary data  $\tau, \ell$  and bulk characteristics  $s, \rho$  of the ETEBA geodesic are more complicated as compared with formula (2.4), (2.5), but admit the explicit form

$$\frac{\tau}{z_h} = \operatorname{arccoth} \left( \frac{-c\kappa^2 + 2c\rho^2 + c + 2\Delta\rho}{2c\rho + 2\Delta} \right), \quad (2.17)$$

$$\ell = \ell_+ + \ell_-, \quad (2.18)$$

### C. Different regimes in equilibration

The regime which we consider are specified by the ratio of  $\ell/z_h$ ,  $\tau/z_h$  and  $\tau/\ell$ . It is interesting that the choice of the regime does not depend on  $\ell/z_H$ ,  $\tau/z_H$ , but the scaling parameters in these regimes do depend on  $z_h/z_H$ , see Section IV. One can study

- *Pre-local-equilibration growth* regime with small  $\tau$ .
  - Both  $\tau$  and  $\ell$  are small
 
$$\tau < \ell < z_h \quad (2.25)$$
  - Only  $\tau$  is small and  $\ell$  is large
 
$$\tau < z_h < \ell \quad (2.26)$$
- *Memory loss*. Both  $\tau$  and  $\ell$  are larger then  $z_h$ 

$$z_h \ll \tau \leq \ell. \quad (2.27)$$

Depending on the ratio of  $\ell - t$  to  $\ell$ ,  $\tau$ ,  $z_h$  there are the following more detailed cases

- *saturation* regime:
 
$$\ell - \tau \ll z_h \quad (2.28)$$
- *late-time memory loss* regime:
 
$$\ell \gg \ell - \tau \gg z_h \quad (2.29)$$
- *Post-local-equilibration linear growth* regime with large  $\ell$ 

$$z_h \ll \tau \ll \ell, \quad (2.30)$$

and therefore,  $\ell - \tau \sim \ell$

### D. Scaling characteristics of thermalization regimes

Characteristics of different regimes during thermalization have been studied in numerous studies [27, 31, 32, 37, 42], and in more details in the paper by H.Lui and J.Sui [20]. In this paper different models have been studied and as one can see from these studies that the main properties are already seen in 1+1 example, described in sect.A. To mention possible generalizations of our result to arbitrary dimension, see VI, below we remind their results for  $d$ -dimensional case. According to these studies in the pre-local-equilibration growth regime the entanglement entropy grows as

$$\Delta S_\Sigma(\tau) = \frac{\pi}{d-1} \mathcal{E} A_\Sigma \left( \frac{\tau}{z_h} \right)^2 + \dots, \quad (2.31)$$

where  $\mathcal{E}$  is the energy density and  $A_\Sigma$  is the area of  $\Sigma$ . This result is independent of the shape of  $\Sigma$ , the spacetime dimension  $d$ , and the specific form of  $h(z)$  [27, 37, 42].

In the memory loss regime

$$S(\ell, \tau) - S_{\text{eq}}(\ell) = -s_{\text{eq}} \lambda(t_s(\ell) - \tau), \quad (2.32)$$

i.e.  $\Delta S(\ell, \tau)$  depends only on the difference  $t_s(\ell) - \tau$ , and not on  $\tau$  and  $\ell$  separately. Here  $\lambda$  is some function that depends on  $h(z)$  and which can be determined explicitly only for  $d = 2$  case, eq.(2.34) below,

$$\lambda(y) = [y + z_h \log(\sin \chi^{-1}(y/z_h))] , \quad (2.33)$$

with  $y = \ell - \tau$  and

$$\chi(\phi) = \left( \cot \frac{\phi}{2} - 1 \right) + \log \tan \frac{\phi}{2}. \quad (2.34)$$

Note  $\lambda(y)$  interpolates between the linear behavior for large  $y/z_h$  and the critical behavior  $y^{\frac{3}{2}}$  near saturation

---


$$\rho_* = \frac{1}{2} \mathcal{V}(\kappa, \phi), \quad (3.1)$$

where we define

$$\mathcal{V}(\kappa, \phi) \equiv 1 + (1 - \mathcal{Q}) \csc \phi, \quad (3.2)$$

$$\mathcal{Q}(\kappa, \phi) \equiv \sqrt{(1 - 2\kappa^2) \cos^2 \phi + 2\kappa^2(1 - \sin \phi)}. \quad (3.3)$$

Substituting (3.1) into (2.17) and (2.19) one can check, that  $\tau$  and  $\ell_+$  are equal to infinity on the critical line.

as  $y/z_h \rightarrow 0$ . For  $d = 2$ , the behaviour (2.32) has been observed also in [16, 42].

Formula (2.32) interpolates between the post-local-equilibration linear growth

$$\Delta S_\Sigma(t) = v_E s_{\text{eq}} A_\Sigma \frac{\tau}{z_h} + \dots \quad (2.35)$$

and the saturation regime,  $t_s - \tau \ll z_h$ ,

$$S(\ell, \tau) - S^{(\text{eq})}(\ell) \propto -\left(\frac{t_s - \tau}{z_h}\right)^\gamma, \quad \gamma = \frac{d+1}{2}. \quad (2.36)$$

In (2.35)  $v_E$  is a dimensionless number which is *independent* of the shape of  $\Sigma$ , but does depend on the final equilibrium state  $s_{\text{eq}} = c/(6z_h)$  and in the particular case  $d=2$   $v_E = 1$ .

Note that in the saturation regime the evolution is beyond the linear regime and it depends on the shape, the spacetime dimension  $d$ , and may also depend on the final equilibrium state [20]. In particular case of 1+1, the saturation time is

$$t_s = \ell + o(\ell), \quad (2.37)$$

The richer structure of the saturation regime takes place in higher dimensions and in the case of RN and Kerr black holes [26, 27].

### III. CRITICAL CURVE

Formulae (2.19) and (2.17) give the explicit dependence for  $\ell$  and  $\tau$  from the geometry of the entanglement surface specified by parameters  $\rho$  and  $\phi$ . For any  $0 \leq \kappa \leq 1$  there is a critical curve in the parameter space  $\rho$  and  $\phi$ , so that only on the right of this line (the red line in Fig.2) one can perform the change of variables  $(\rho, \phi) \rightarrow (\ell, \tau)$ . To visualize this change of variables it is convenient to draw the lines of fixed values of  $\ell$  and  $\tau$  (brown and blue lines in Fig.2). From Fig.2 we see that large values of  $\ell$  and  $\tau$  are located near the critical line. The explicit form of the critical line  $\rho = \rho_*(\phi)$  is defined by the following formula

---

Near the critical line we have

$$\frac{-c\kappa^2 + 2c\rho^2 + c + 2\rho\sqrt{\rho^2 - \kappa^2}}{2c\rho + 2\sqrt{\rho^2 - \kappa^2}} \Big|_{\rho=\rho_*+\epsilon} = 1 + 2\epsilon \mathcal{K}_\tau(\phi, \kappa) + \mathcal{O}(\epsilon^2), \quad (3.4)$$

where

$$\mathcal{K}(\kappa, \phi) = \frac{c^2 \Delta (\kappa^2 + 2\rho^2 - 1) + c\rho (-3\kappa^2 + 4\rho^2 - 1) + 2\Delta^3}{4\Delta(c\rho + \Delta)^2} \Big|_{\rho=\rho_*}, \quad (3.5)$$

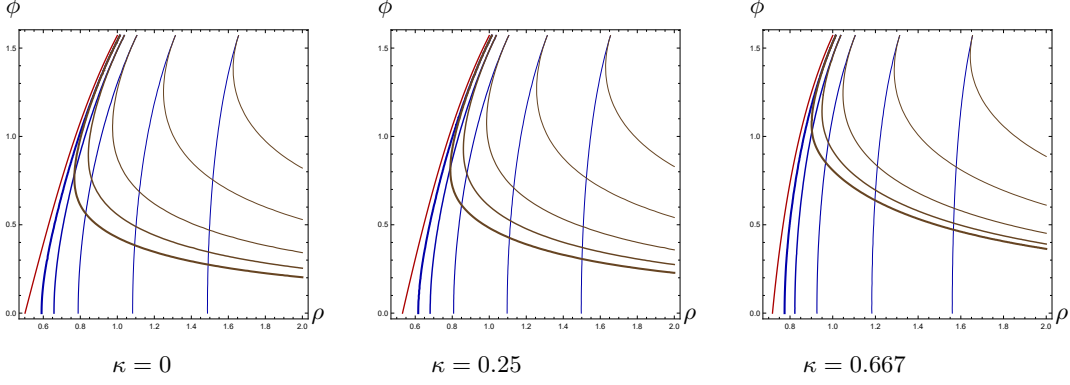


FIG. 2. The contour plots for  $\ell$  and  $\tau$  as functions of  $\rho$  and  $\phi$  for different  $\kappa = 0, 0.25$  and  $0.667$ . These plots show that in the left of the critical line (the darker red line) for  $\ell > \tau$  we can always find solution to the system of equations:  $\tau = \tau(\rho, \phi); \ell = \ell(\rho, \phi)$ . Lines of the equal times  $\tau = 0.7, 1, 1.5, 2, 2.5$  in all panels are shown by blue color with increasing thickness from right to left. Lines of the equal  $\ell = 0.7, 1, 1.5, 2, 2.5$  in all panels are shown by brown with increasing thickness from up to bottom.

and, therefore, we get near the critical curve the following time asymptotic

$$\tau = -\frac{z_h}{2} \log \varepsilon - \frac{z_h}{2} \log \mathcal{K} + \mathcal{O}(\varepsilon). \quad (3.6)$$

The same expansion for  $\ell_+$  is

$$\ell_+ = -\frac{z_h}{2} \log \varepsilon + \frac{z_h}{2} \log \mathcal{K}^+ + \mathcal{O}(\varepsilon), \quad (3.7)$$

where

$$\mathcal{K}^+ = \frac{\mathfrak{N}}{\mathfrak{K}}, \quad (3.8)$$

and

$$\mathfrak{K} = 2\sqrt{2} \mathcal{Q} \sin \phi - 4 \cos^2 \phi + 4\kappa^2 (2 \sin \phi (1 - \sin \phi) - \mathcal{Q}), \quad (3.9)$$

$$\mathfrak{N} = 4(\kappa^2 - 1)^2 \cos^2 \phi - \frac{(\mathcal{V}^2 - 4\kappa^2)((\mathcal{V}^2 - 8) \sin^2 \phi + 4)}{4} + \frac{1}{2} \sqrt{\mathcal{V}^2 - 4\kappa^2} (\mathcal{V}^2 - 2(\kappa^2 + 1)) \sin(2\phi), \quad (3.10)$$

where  $\mathcal{V}$  and  $\mathcal{Q}$  are defined by (3.2) and (3.3), respectively.

The expression for  $\ell_-$  is not singular on the critical line

$$\ell_- = \frac{z_h}{2\kappa} \log \mathcal{K}^-, \quad (3.11)$$

and

$$\mathcal{K}^- = \frac{2 \sin \phi \sqrt{\mathcal{V}^2 - 4\kappa^2} + 4\kappa \cos \phi}{\mathcal{V}^2 \sin^2 \phi - 4\kappa^2}. \quad (3.12)$$

In the limit of  $\kappa \rightarrow 0$  we have

$$\mathcal{K}(\kappa, \phi) \xrightarrow{\kappa \rightarrow 0} 1 + \cot \frac{\phi}{2}, \quad (3.13)$$

$$\mathcal{K}^+(\kappa, \phi) \xrightarrow{\kappa \rightarrow 0} \frac{\cot \frac{\phi}{2} + 1}{\cot \frac{\phi}{2}}, \quad (3.14)$$

$$\mathcal{K}^-(\kappa, \phi) \underset{\kappa \sim 0}{\approx} 1 + 2\kappa (\cot \frac{\phi}{2} - 1). \quad (3.15)$$

#### IV. MEMORY LOSS REGIME IN NON-EQUILIBRIUM HEATING

Using formulae (3.6), (3.11) and (3.7) we get, that near the critical curve the difference

$$T_- \equiv \frac{\tau - \ell}{z_h} \quad (4.1)$$

is finite and can be expressed in the form

$$T_- = -\chi_\kappa(\phi), \quad (4.2)$$

where function  $\chi_\kappa$  is defined as

$$\chi_\kappa(\phi) \equiv -\frac{1}{2} \log \mathcal{K}(\kappa, \phi) \mathcal{K}^+(\kappa, \phi) - \frac{1}{2\kappa} \log \mathcal{K}^-(\kappa, \phi). \quad (4.3)$$

The second lightcone variable,

$$T_+ \equiv \tau/z_h + \ell/z_h, \quad (4.4)$$

is singular near the critical line

$$T_+ \sim -\log \varepsilon. \quad (4.5)$$

The function  $\chi_\kappa(\phi)$  plays an important role in what follows, controlling the behaviour of the lightcone variable  $T_-$ . In the limit  $\kappa \rightarrow 0$  we have

$$\chi_\kappa(\phi) \xrightarrow{\kappa \rightarrow 0} \chi_0(\phi), \quad (4.6)$$

where  $\chi_0(\phi) = \cot \frac{\phi}{2} - 1 - \log \cot \frac{\phi}{2}$  in accordance with (2.34). The inverse function  $\chi^{-1}$  can be expressed in terms of Lambert function  $W$

$$\phi = \chi_0^{-1}(T_-) = 2 \operatorname{arccot}(-W_{-1}(-e^{T_- - 1})). \quad (4.7)$$

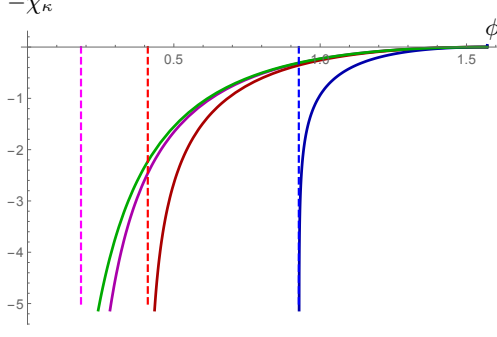


FIG. 3. The plot of functions  $-\chi_\kappa(\phi)$  (solid lines) for different  $\kappa$ . The vertical dashed lines correspond to  $\phi = \vartheta_\kappa$  for corresponding  $\kappa$ . The magenta lines correspond to  $\kappa = 0.1$ , darker red line to  $\kappa = 0.25$  and blue lines to  $\kappa = 0.667$ . The green line represents  $-\chi_0(\phi)$ .

Now let us consider the entanglement entropy behaviour near the critical line

$$\begin{aligned} S - S_{eq} &= \log \frac{1}{\mathfrak{S}} \frac{\sinh \frac{\tau}{z_h}}{\sinh \frac{\ell}{z_h}} \\ &\approx \frac{\tau - \ell}{z_h} - 2 \sinh \frac{\tau - \ell}{z_h} e^{-\frac{\tau + \ell}{z_h}} - \log \mathfrak{S}(\phi, \rho_H^*, \kappa). \end{aligned} \quad (4.8)$$

Note, that  $\mathfrak{S}(\phi, \rho, \kappa)$  is not singular on the critical line. Neglecting the exponentially small terms in (4.8) and introducing  $\mathfrak{S}_\kappa(\phi) = \mathfrak{S}(\phi, \rho_H^*, \kappa)$  we get

$$\Delta S \equiv S - S_{eq} \approx T_- - \log \mathfrak{S}_\kappa(\phi). \quad (4.9)$$

Formula (4.2) gives the representation of  $\phi$  in term of  $T_-$

$$\phi = \chi_\kappa^{-1}(-T_-), \quad (4.10)$$

and we get that near the critical line the entanglement entropy has the wave spreading

$$\Delta S \approx T_- - \log \mathfrak{S}_\kappa(\chi_\kappa^{-1}(-T_-)). \quad (4.11)$$

The dependence of entanglement entropy propagation only on  $T_-$ , i.e. realization of the memory loss regime, is based on the exponential suppression of  $T_+$  dependence, see (4.8), and dependence of  $\mathfrak{S}$  only on  $\phi$  near the critical line.

#### A. Saturation. Expansion near $\pi/2$

One of limiting forms of memory loss regime is called the saturation regime and it corresponds to  $T_- \rightarrow -0$ . This corresponds to time scales near the final equilibration time  $t_s \approx \ell$ . In parametric space it corresponds to the values  $\phi \rightarrow \pi/2$ .

Let us consider asymptotics of  $\tau$ ,  $\ell_-$  and  $\ell_+$  given by (3.7), (3.11) and (3.6) when  $\phi \rightarrow \pi/2$

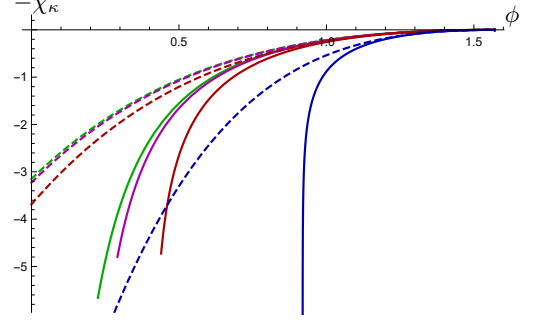


FIG. 4. The plot of  $-\chi_\kappa(\phi)$  (solid lines) for different  $\kappa$  compared with the approximate formula (4.13) (dashed lines) near  $\phi = \pi/2$ . The green lines correspond to  $\kappa = 0$ , the magenta lines to  $\kappa = 0.1$ , darker red line to  $\kappa = 0.25$  and the blue lines to  $\kappa = 0.667$ .

$$\begin{aligned} \frac{\tau}{z_h} &\approx -\frac{\log \varepsilon}{2} + \frac{\log 2}{2} + \frac{(\frac{\pi}{2} - \phi)}{4\sqrt{1 - \kappa^2}} + \frac{(-1 + 2\kappa^2)(\phi - \frac{\pi}{2})^2}{32(-1 + \kappa^2)}, \\ \frac{\ell_-}{z_h} &\approx \frac{(\frac{\pi}{2} - \phi)}{\sqrt{1 - \kappa^2}} + \frac{(\phi - \frac{\pi}{2})^2}{2(1 - \kappa^2)}, \\ \frac{\ell_+}{z_h} &\approx -\frac{\log \varepsilon}{2} + \frac{\log 2}{2} + \frac{3(\frac{\pi}{2} - \phi)}{4\sqrt{1 - \kappa^2}} + \frac{(-1 + 2\kappa^2)(\phi - \frac{\pi}{2})^2}{16(-1 + \kappa^2)}. \end{aligned} \quad (4.12)$$

and we have (we compare this formula with exact one in Fig.5)

$$\begin{aligned} \frac{\ell - \tau}{z_h} &= \chi_\kappa(\phi) \approx \\ &\frac{z_h \delta^2}{2(1 - \kappa^2)} + \frac{(z_h + 2\kappa^2 z_h) \delta^3}{6(1 - \kappa^2)^{3/2}} - \frac{(5z_h + 7\kappa^2 z_h) \delta^4}{24(1 - \kappa^2)^2(1 + \kappa^2)}. \end{aligned} \quad (4.13)$$

where  $\delta \approx \pi/2 - \phi$ .

The inverse function  $\chi_\kappa^{-1}$  is expressed in the form

$$\begin{aligned} \delta &\approx -\sqrt{2(1 - \kappa^2)} \left( \frac{\ell - \tau}{z_h} \right)^{1/2} + \frac{\sqrt{1 - \kappa^2}(1 + 2\kappa^2)}{3} \frac{\ell - \tau}{z_h} \\ &\quad - \frac{(20\kappa^4 - \kappa^2 - 10)\sqrt{1 - \kappa^2}}{18\sqrt{2}} \left( \frac{\ell - \tau}{z_h} \right)^{3/2}. \end{aligned} \quad (4.14)$$

Finally, expanding  $\log \mathfrak{S}$  near  $\phi \rightarrow \pi/2$

$$\log \mathfrak{S} \approx \frac{\delta^2}{2(1 - \kappa^2)} + \quad (4.15)$$

$$\frac{\kappa^2 \delta^3}{2(1 - \kappa^2)^{3/2}} + \frac{(2 + 7\kappa^2 + 3\kappa^4) \delta^4}{24(1 - \kappa^2)^2}, \quad (4.16)$$

we get

$$\begin{aligned} \Delta S &\approx -f_\kappa \left( \frac{\ell - \tau}{z_h} \right)^{3/2} - n_\kappa \left( \frac{t_s - \tau}{z_h} \right)^2 \\ f_\kappa &= \frac{(\sqrt{2}(1 - \kappa^2))}{3}, \quad n_\kappa = \frac{(1 - \kappa^2)^2}{6}. \end{aligned} \quad (4.17)$$

We see that there is essential dependence of the coefficient  $f_\kappa$  in front of scaling law on the initial temperature. Note, that at  $\kappa = 1$  all the expansion for saturation regime vanishes identically.

### B. Post-local-equilibration linear growth. Expansion near $\vartheta_\kappa$

First let us consider  $\ell_-$ . The new feature of behaviour of  $\ell_-$  for  $\kappa > 0$ , is that it is singular near  $\phi = \vartheta_\kappa$ ,

$$\vartheta_\kappa = \arccos \left( \frac{\sqrt{1+2\kappa-3\kappa^2}}{\sqrt{1+2\kappa+\kappa^2}} \right). \quad (4.18)$$

When  $\phi = \vartheta_\kappa + \delta$  we get

$$\frac{\ell_-}{z_h} \approx -\frac{\log \delta}{2\kappa} + \zeta_\kappa^-, \quad (4.19)$$

where

$$\zeta_\kappa^- = \frac{1}{2\kappa} \log \left( \frac{4\kappa(-2\kappa^2 + \kappa + 1)}{(\kappa + 1)^2 \sqrt{(2-3\kappa)\kappa + 1}} \right). \quad (4.20)$$

Since time  $\tau$  and  $\ell_+$  are not singular near this point we get

$$-T_- \equiv \ell - \tau = \chi_\kappa(\vartheta_\kappa + \delta) = -\frac{1}{2\kappa} \log \delta + \zeta_\kappa, \quad (4.21)$$

$$\zeta_\kappa = \zeta_\kappa^- + \frac{1}{2} \log \frac{\kappa^2}{(1+\kappa)^2}. \quad (4.22)$$

Using the following properties of factors defined  $\mathfrak{S}$ , see equation (2.16),

$$\mathfrak{S}_\kappa(\rho, s) = \frac{c\rho + \Delta}{\Delta} \cdot \sqrt{\frac{\Delta^2 - c^2\rho^2}{\rho(c^2\rho + 2c\Delta + \rho) - \kappa^2}}, \quad (4.23)$$

$$\frac{\Delta}{c\rho + \Delta} \Big|_{\rho=\rho_{cr}, \phi=\vartheta_\kappa} = \frac{1}{2}, \quad (4.24)$$

$$\Delta^2 - c^2\rho^2 \Big|_{\rho=\rho_{cr}, \phi=\vartheta_\kappa+\delta} = \mathfrak{q}_\kappa^2 \delta, \quad (4.25)$$

$$\rho(c^2\rho + 2c\Delta + \rho) - \kappa^2 \Big|_{\rho=\rho_{cr}, \phi=\vartheta_\kappa} = \mathfrak{r}_\kappa^2, \quad (4.26)$$

where

$$\mathfrak{q}_\kappa^2 = \begin{cases} 0.16\delta & \text{for } \kappa = 0.1 \\ 0.39\delta & \text{for } \kappa = 0.25 \\ 0.86\delta & \text{for } \kappa = 0.66, \end{cases} \quad (4.27)$$

$$\mathfrak{r}_\kappa^2 = 1.331 - 3(\kappa - 0.334)^2, \quad (4.28)$$

we get that near the critical line and when  $\phi \approx \vartheta_\kappa + \delta$

$$\mathfrak{S}_\kappa(\rho, s) \Big|_{\rho=\rho_{cr}, \phi=\vartheta_\kappa+\delta} = \frac{2\mathfrak{q}_\kappa}{\mathfrak{r}_\kappa} \delta^{1/2}. \quad (4.29)$$

Hence

$$\Delta S \approx T_- - \log \frac{2\mathfrak{q}_\kappa}{\mathfrak{r}_\kappa} e^{-\kappa(-T_- - \zeta_\kappa)} \quad (4.30)$$

$$= (1 - \kappa)T_- - \kappa\zeta_\kappa - \log \frac{2\mathfrak{q}_\kappa}{\mathfrak{r}_\kappa}. \quad (4.31)$$

Therefore, the linear coefficient is changed as compare to the case of the initial zero temperature, and

$$\mathfrak{k}_\kappa = 1 - \kappa, \quad (4.32)$$

that is in agreement with numerical calculations presented in Fig. 7.

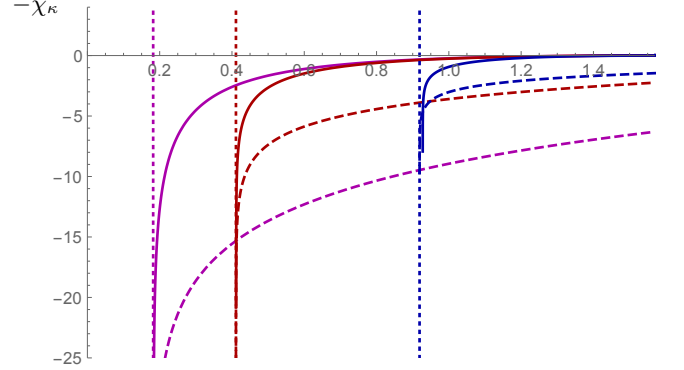


FIG. 5. The plot of  $-\chi_\kappa(\phi)$  (solid lines) for different  $\kappa$  compared with the approximate formula (4.21),(4.22) (dashed lines) near  $\phi = \vartheta_\kappa$ . The magenta lines correspond to  $\kappa = 0.1$ , darker red line to  $\kappa = 0.25$  and blue lines to  $\kappa = 0.667$ .

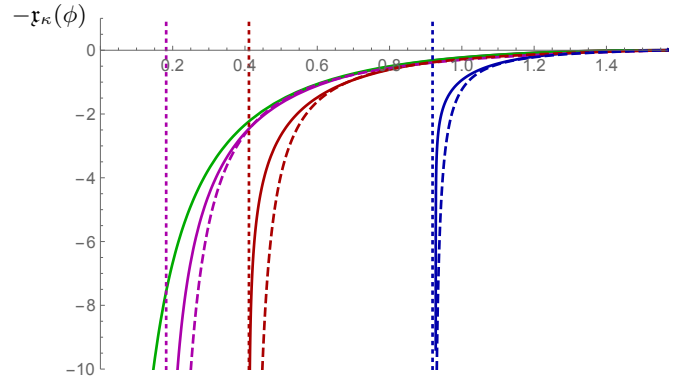


FIG. 6. The plots of the best fit  $-\mathfrak{r}_\kappa(\phi)$  (dashed lines) given by (4.33) compare to the exact  $-\chi_\kappa(\phi)$  (solid lines) at different  $\kappa$ . The magenta lines correspond to  $\kappa = 0.1$ , darker red lines to  $\kappa = 0.25$  and blue lines to  $\kappa = 0.667$ . The green line represents  $-\chi_0(\phi)$ .

### C. Late-time memory loss regime.

### Interpolation between $\phi = \vartheta_\kappa$ and $\pi/2$

As interpolation functions  $\mathfrak{x}_\kappa(\phi)$  to  $\chi_\kappa(\phi)$  on the interval  $(\vartheta_\kappa, \pi/2)$  we take, see Fig.6,

$$\mathfrak{x}_\kappa = a_\kappa \left( \cot \frac{\phi - \vartheta_\kappa}{2b_\kappa} - \cot \frac{\frac{\pi}{2} - \vartheta_\kappa}{2b_\kappa} - \log \frac{\cot \frac{\phi - \vartheta_\kappa}{2b_\kappa}}{\cot \frac{\frac{\pi}{2} - \vartheta_\kappa}{2b_\kappa}} \right), \quad (4.33)$$

where the numerical values of  $a_\kappa$  and  $b_\kappa$  are

$$\begin{aligned} a_{0.1} &= 0.15, & b_{0.1} &= 2.5, \\ a_{0.25} &= 0.07, & b_{0.25} &= 2.8, \\ a_{0.667} &= 0.014, & b_{0.667} &= 3.8. \end{aligned} \quad (4.34)$$

The inverse functions to  $\mathfrak{x}_\kappa$  are given by

$$\mathfrak{x}_\kappa^{-1} \equiv \phi = \vartheta_\kappa + 2b_\kappa \operatorname{arccot} W_{-1} \left( -e^{-\frac{\mathfrak{x}_\kappa}{a_\kappa} - \cot \phi_{\kappa,0}} \cot \phi_{\kappa,0} \right), \quad (4.35)$$

where

$$\phi_{\kappa,0} \equiv \frac{\frac{\pi}{2} - \vartheta_\kappa}{2b_\kappa}. \quad (4.36)$$

Substituting (4.35) to (4.30) we get

$$\Delta S \approx T_- - \log \mathfrak{S}_\kappa \left( \vartheta_\kappa + 2b_\kappa \operatorname{arccot} W_{-1} \left( -e^{-\frac{\mathfrak{x}_\kappa}{a_\kappa} - \cot \phi_{\kappa,0}} \cot \phi_{\kappa,0} \right) \right). \quad (4.37)$$

From Fig. 7 we see that in the region of large of  $L \equiv -T_-$  we have the linear growth of  $\Delta S$ .

## V. NUMERICAL RESULTS

In the previous sections we have shown, that for some values of  $\tau$  and  $\ell$  the function  $\Delta S$  depends only on their difference  $\tau - \ell$ . From Fig.9 we see that for large values of  $\ell$  and  $\tau$  and  $\ell > \tau$ , the function  $\Delta S(z_H, \ell, \tau)$  in fact depends only on the  $T_-$  light-cone variable

$$T_- = \tau - \ell, \quad (5.1)$$

and the dependence on  $\ell$  is negligible away from the line  $T_- = -\ell$ , i.e. for large times, and for large length  $\ell$ . Also this effect is presented in coordinates  $\ell$  and  $\tau$  in the top panels in Fig.9. It is instructive to present the dependence on  $T_-$  in the 2D plot keeping  $\ell$  fixed, see Fig.8.

In Fig.8 we present the explicit dependence of  $\Delta S(z_H, \ell, T_- + \ell)$  on  $T_-$  for the different values of  $\kappa$  and for different values of  $\ell$ . Solid lines corresponding

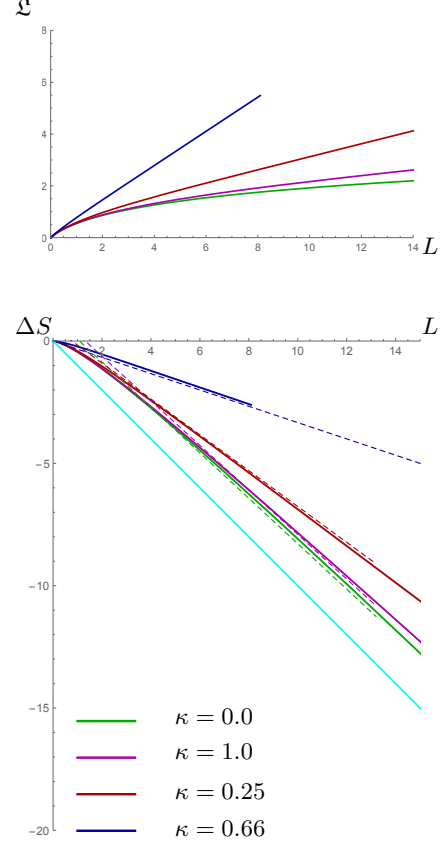


FIG. 7. The plot of functions  $\mathfrak{L}(L) = -\log \mathfrak{S}_\kappa(\chi_\kappa^{-1}(+L))$  and  $\Delta S$  as function on  $L$  for  $\kappa = 0.66, 0.25, 0.1, 0$ , the blue, red, magenta and green solid lines, respectively. We see the linear dependence of  $\Delta S$  on  $L$  for large  $L$  with the slope equal to  $\mathfrak{x}_\kappa$ . The values of  $\mathfrak{x}_\kappa = 0.34, 0.75, 0.9, 1$ , for  $\kappa = 0.66, 0.25, 0.1, 0$  respectively the blue, red, magenta and green dashed lines respectively. The cyan line is a test line with the slope equal to 1.

to  $\kappa = 0.25$  in the bottom panel of Fig.8 shows strong deviation from dotted lines corresponding to  $\kappa = 0$  for large enough  $T_-$ . Also in Fig.8 one can see that for larger values of  $\ell$  function  $\Delta S$  for  $\kappa = 0$  tends to be closer to the red line in the bottom panel. The middle panel of Fig.8 shows, that the larger values of  $\ell$  for different  $\kappa$  make the dependence closer to the linear (see dotted and solid lines in this panel) for large enough  $T_-$ .

## VI. CONCLUSIONS AND DISCUSSIONS

In this paper we considered the evolution of entanglement entropy during equilibration after the global quench of an initial thermal state at temperature  $T_i$  followed by non-equilibrium heating to temperature  $T_f$ , in an example of the simplest quenched holographic model. In the bulk this equilibration process is described by the Vaidya



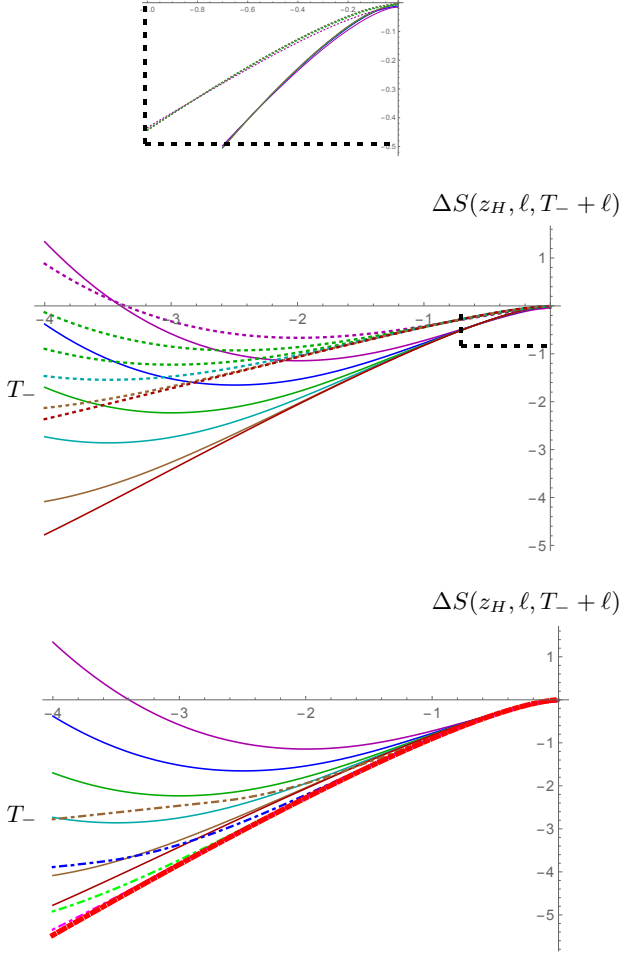


FIG. 8. The plot of the dependence of  $\Delta S(z_H, \ell, T_- + \ell)$  on  $T_-$  for  $\ell$  fixed and equal to 3, 4, 5, 6, 7, 9, 12;  $z_H = 1.5$ ,  $z_h = 1$  (dotted lines),  $z_H = 4$ ,  $z_h = 1$  (solid lines),  $z_H = \infty$ ,  $z_h = 1$  (dot-dashed lines). The red line represent  $\Delta S(\infty, \ell, T_- + \ell)$  given by (2.33).

shell in the black hole background. This is in contrast to the Vaidya shell in the AdS background, that corresponds to thermalization. In both cases the holographic entanglement entropy is defined as the area of an extremal surface anchored on a given area on the boundary.

Using the explicit representation for the evolution of the holographic entanglement entropy we have shown the existence of the memory loss regime in equilibration process started from a thermal state and followed by non-equilibrium increasing of the temperature. The memory loss regime occurs long after the system has achieved local equilibration at scales of order  $z_h$  and the holographic entanglement entropy evolution in this regime is described by the function depending only on one variable

$$\Delta S(\ell, \tau) \approx \mathfrak{M}_\kappa(\ell - \mathfrak{v}\tau), \quad (6.1)$$

for our simplest model  $\mathfrak{v} = 1$ . The form of the function in the LHS of (6.1) depends on  $\kappa$ . As for the thermalization

model [20], there are two special cases of the memory loss regime, namely

- *Post-local-equilibration linear growth* regime with large  $\ell$ ,  $z_h \ll \tau \ll \ell$ ,  $\ell - \tau \sim \ell$

$$\mathfrak{M}_\kappa(\ell - \tau) \approx -\mathfrak{k}_\kappa(\ell - \tau) + \dots \quad (6.2)$$

where the scaling parameter  $\mathfrak{k}_\kappa$  depends on  $\kappa$  as  $\mathfrak{k}_\kappa = 1 - \kappa$ ;

- *saturation* regime,  $\ell - \tau \ll z_h$ ,

$$\mathfrak{M}_\kappa(\ell - \tau) \approx -\mathfrak{f}_\kappa \left( \frac{\ell - \tau}{z_h} \right)^{3/2} + \dots \quad (6.3)$$

where the scaling parameter  $\mathfrak{f}_\kappa$  depends on  $\kappa$  as  $\mathfrak{f}_\kappa = \frac{\sqrt{2}}{3} (1 - \kappa^2)$ .

For more complicated model we expect that the form of the function  $\mathfrak{M}_\kappa$  depends on the model, but the dependence on  $(\ell - \mathfrak{v}\tau)$  will survive for more general initial states, changing only the value of  $\mathfrak{v}$ . In particular, for the linear growth regime we expect that the speed  $\mathfrak{v}$ , characterizing properties of the equilibrium state, is solely determined by the metric of the black hole describing the final state. The form (6.1) manifests itself the local nature of entanglement propagation.

Note, that the 3/2 law in saturation regime exhibits also the temporal evolution of causal holographic information [37].

Let us also note, that the pre-local-equilibration stage in non-equilibrium heating is very similar to the one during thermalization. As has been noticed in [21] the pre-local-equilibration stage in thermalization is rather sensitive to the nature of initial states, including the value of the sourcing interval  $\delta t$ . In our case the early growth time dependence is proportional to the difference of the energy densities

$$\Delta S = 2\pi (\mathcal{E}_f - \mathcal{E}_i) \tau^2 + \dots, \quad (6.4)$$

that is consistent with studies of the entanglement entropy of excited states at  $T_i = 0$  in [20, 21, 43–46].

We have considered 1+1 dimension case, but using explicit integral representations for the holographic entanglement entropy and the others nonlocal observables for higher dimensional cases describing the non-equilibrium heating, one can derive, similar to the case of holographic thermalization process [21], general scaling behaviour in the corresponding boundary theories during instantaneous heating.

It is interesting to consider non-equilibrium heating process initiated by more general quenches, in particular those with inhomogeneous states, compare with [47–49], as well to consider different infalling shells, in particular massive infalling shells, charged shells and shells with angular momentum, corresponding thermalization process have been studied in [5, 50–53], [28, 29] and in [19], respectively, as well as the case of corresponding thick

shells. Thick shells infalling in black hole background in higher dimensional cases have been already used to study numerically the holographic non-equilibrium heating [18]. When the thickness of the shell is less than typical sizes of intervals which we deal with, the evolution of

the entanglement entropy for large intervals also shows the memory loss regime numerically, the wave front of entanglement develop also a finite spread and the picture is similar to the thermalization picture, but the corresponding wave amplitudes  $\mathfrak{M}$  are suppressed as the initial temperature increases.

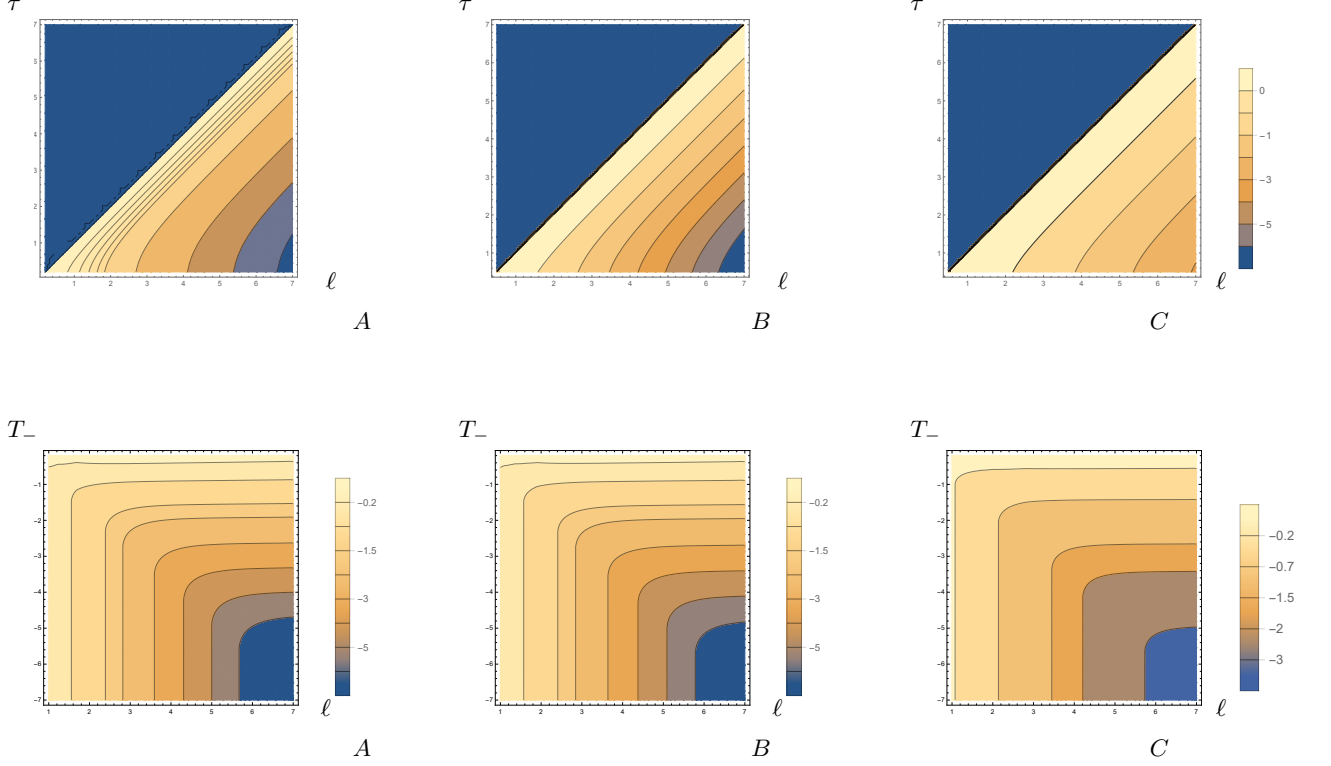


FIG. 9. **Top:** Contour plot for  $\Delta S(\ell, \tau)$ . We see the wave character of the exact  $\Delta S(\tau, \ell) = S - S_{eq}$  for large  $\tau, \ell$ . The contour plot of  $\Delta S(\ell, \tau)$ : A)  $z_H = 4, z_h = 1$ ; B)  $z_H = 1.5, z_h = 1$ . **Bottom:** The contour plot of  $\Delta S(\ell, T_- + \ell)$  as function of  $\ell$  and  $T_-$ . A.  $z_H = \infty$ , B.  $z_H = 4$ , C.  $z_H = 1.5$ . We see the wave character of the exact  $\Delta S(\ell, \tau) = S - S_{eq}$  for large  $\tau$  and  $\ell$ .

## ACKNOWLEDGEMENTS

The authors are grateful to M. Khramtsov for useful discussions. This work is supported by the Russian Sci-

ence Foundation (project 14-50-00005, Steklov Mathematical Institute).

- [1] J. M. Maldacena, “The Large N limit of superconformal field theories and supergravity,” *Int. J. Theor. Phys.* **38**, 1113 (1999) [*Adv. Theor. Math. Phys.* **2**, 231 (1998)] [*hep-th/9711200*].
- [2] S. S. Gubser, I. R. Klebanov, A. M. Polyakov, “Gauge theory correlators from noncritical string theory,” *Phys. Lett. B* **428**, 105-114 (1998) [*hep-th/9802109*].
- [3] E. Witten, “Anti-de Sitter space and holography,” *Adv. Theor. Math. Phys.* **2**, 253-291 (1998) [*hep-th/9802150*].
- [4] E. Witten, “Anti-de Sitter space, thermal phase transition, and confinement in gauge theories,” *Adv. Theor. Math. Phys.* **2**, 505 (1998) [*hep-th/9803131*].
- [5] U. H. Danielsson, E. Keski-Vakkuri and M. Kruczenski, “Black hole formation in AdS and thermalization on the boundary,” *JHEP* **0002**, 039 (2000) [*hep-th/9912209*].
- [6] J. M. Maldacena, “Eternal black holes in anti-de Sitter,” *JHEP* **0304**, 021 (2003) [*hep-th/0106112*].

- [7] P. Calabrese and J. L. Cardy, “Evolution of entanglement entropy in one-dimensional systems,” *J. Stat. Mech.* **0504**, P04010 (2005) [cond-mat/0503393];
- [8] P. Calabrese and J. Cardy, “Time-dependence of correlation functions following a quantum quench,” *Phys. Rev. Lett.* **96** 13680 (2006); arXiv:cond-mat/0601225.
- [9] I. Ya. Aref’eva, “Holographic approach to quark-gluon plasma in heavy ion collisions,” *Phys. Usp.* **57**, 527 (2014).
- [10] O. DeWolfe, S. S. Gubser, C. Rosen and D. Teaney, “Heavy ions and string theory,” *Prog. Part. Nucl. Phys.* **75**, 86 (2014) [arXiv:1304.7794 [hep-th]].
- [11] J. Casalderrey-Solana, H. Liu, D. Mateos, K. Rajagopal, U. A. Wiedemann, “Gauge/String Duality, Hot QCD and Heavy Ion Collisions,” [arXiv:1101.0618 [hep-th]].
- [12] S. A. Hartnoll, “Lectures on holographic methods for condensed matter physics,” *Class. Quant. Grav.* **26**, 224002 (2009) [arXiv:0903.3246 [hep-th]].
- [13] R. Easther, R. Flauger, P. McFadden and K. Skenderis, “Constraining holographic inflation with WMAP,” *JCAP* **1109**, 030 (2011) [arXiv:1104.2040 [astro-ph.CO]].
- [14] V. Balasubramanian *et al.*, “Holographic Thermalization,” *Phys. Rev. D* **84**, 026010 (2011) [arXiv:1103.2683 [hep-th]].
- [15] J. Aparicio and E. Lopez, “Evolution of Two-Point Functions from Holography,” *JHEP* **1112**, 082 (2011) [arXiv:1109.3571 [hep-th]].
- [16] J. Abajo-Arrestia, J. Aparicio and E. Lopez, “Holographic Evolution of Entanglement Entropy,” *JHEP* **1011**, 149 (2010) [arXiv:1006.4090 [hep-th]].
- [17] T. Hartman and J. Maldacena, “Time Evolution of Entanglement Entropy from Black Hole Interiors,” arXiv:1303.1080 [hep-th].
- [18] I. Ya. Arefeva and I. V. Volovich, I. Ya. Arefeva and I. V. Volovich, “On holographic thermalization,” *Theor. Math. Phys.* **174**, 186 (2013) [*Teor. Mat. Fiz.* **174**, 216 (2013)], arXiv:1211.6041 [hep-th].
- [19] I. Aref’eva, A. Bagrov and A. S. Koshelev, “Holographic Thermalization from Kerr-AdS,” *JHEP* **1307**, 170 (2013) [arXiv:1305.3267 [hep-th]].
- [20] H. Liu and S. J. Suh, “Entanglement Tsunami: Universal Scaling in Holographic Thermalization,” *Phys. Rev. Lett.* **112**, 011601 (2014) [arXiv:1305.7244 [hep-th]].
- [21] H. Liu and S. J. Suh, “Entanglement growth during thermalization in holographic systems,” *Phys. Rev. D* **89**, 066012 (2014), arXiv:1311.1200 [hep-th].
- [22] Y. -Z. Li, S. -F. Wu, Y. -Q. Wang and G. -H. Yang, “Linear growth of entanglement entropy in holographic thermalization captured by horizon interiors and mutual information,” arXiv:1306.0210 [hep-th].
- [23] S. H. Shenker and D. Stanford, “Black holes and the butterfly effect,” arXiv:1306.0622 [hep-th].
- [24] D. S. Ageev and I. Y. Aref’eva, “Waking and Scrambling in Holographic Heating up,” arXiv:1701.07280 [hep-th].
- [25] V. E. Hubeny and H. Maxfield, “Holographic probes of collapsing black holes,” *JHEP* **1403** (2014) 097, [arXiv:1312.6887].
- [26] T. Albash and C. V. Johnson, “Evolution of Holographic Entanglement Entropy after Thermal and Electromagnetic Quenches,” *New J. Phys.* **13**, 045017 (2011) [arXiv:1008.3027 [hep-th]].
- [27] V. Balasubramanian, A. Bernamonti, J. de Boer, N. Copland, B. Craps, E. Keski-Vakkuri, B. Muller and A. Schafer *et al.*, “Thermalization of Strongly Coupled Field Theories,” *Phys. Rev. Lett.* **106**, 191601 (2011) [arXiv:1012.4753 [hep-th]].
- [28] D. Galante and M. Schvellinger, *JHEP* **1207**, 096 (2012) [arXiv:1205.1548 [hep-th]].
- [29] E. Caceres and A. Kundu, “Holographic Thermalization with Chemical Potential,” *JHEP* **1209**, 055 (2012) [arXiv:1205.2354 [hep-th]].
- [30] W. Baron, D. Galante and M. Schvellinger, “Dynamics of holographic thermalization,” *JHEP* **1303**, 070 (2013) [arXiv:1212.5234 [hep-th]].
- [31] V. Keranen, E. Keski-Vakkuri and L. Thorlacius, “Thermalization and entanglement following a non-relativistic holographic quench,” *Phys. Rev. D* **85**, 026005 (2012) [arXiv:1110.5035 [hep-th]].
- [32] P. Fonda, L. Franti, V. Keranen, E. Keski-Vakkuri, L. Thorlacius and E. Tonni, “Holographic thermalization with Lifshitz scaling and hyperscaling violation,” *JHEP* **1408**, 051 (2014) [arXiv:1401.6088 [hep-th]].
- [33] I. Ya. Aref’eva, “Formation time of quark-gluon plasma in heavy-ion collisions in the holographic shock wave model,” *Teor. Mat. Fiz.* **184**, no. 3, 398 (2015) [*Theor. Math. Phys.* **184**, no. 3, 1239 (2015)] [arXiv:1503.02185 [hep-th]].
- [34] I. Ya. Aref’eva, A. A. Golubtsova and E. Gourgoulhon, “Analytic black branes in Lifshitz-like backgrounds and thermalization,” *JHEP* **1609**, 142 (2016) [arXiv:1601.06046 [hep-th]].
- [35] S. Sotiriadis, P. Calabrese and J. Cardy, “Quantum Quench from a Thermal Initial State”, *EPL* (2009) 20002 [arXiv:0903.0895 [cond-mat]].
- [36] I. Aref’eva and I. Volovich, “Holographic Photosynthesis,” arXiv:1603.09107 [hep-th].
- [37] V. E. Hubeny, M. Rangamani and E. Tonni, “Thermalization of Causal Holographic Information,” arXiv:1302.0853 [hep-th].
- [38] Y. -Z. Li, S. -F. Wu, Y. -Q. Wang and G. -H. Yang, “Linear growth of entanglement entropy in holographic thermalization captured by horizon interiors and mutual information,” arXiv:1306.0210 [hep-th].
- [39] S. H. Shenker and D. Stanford, “Black holes and the butterfly effect,” arXiv:1306.0622 [hep-th].
- [40] S. Ryu and T. Takayanagi, “Holographic derivation of entanglement entropy from AdS/CFT,” *Phys. Rev. Lett.* **96**, 181602 (2006) [hep-th/0603001].
- [41] V. E. Hubeny, M. Rangamani and T. Takayanagi, *JHEP* **0707**, 062 (2007) [arXiv:0705.0016 [hep-th]].
- [42] J. Aparicio and E. Lopez, “Evolution of Two-Point Functions from Holography,” *JHEP* **1112**, 082 (2011) [arXiv:1109.3571 [hep-th]].
- [43] D. Allahbakhshi, M. Alishahiha and A. Naseh, “Entanglement Thermodynamics,” arXiv:1305.2728 [hep-th].
- [44] J. Bhattacharya, M. Nozaki, T. Takayanagi and T. Ugajin, “Thermodynamical Property of Entanglement Entropy for Excited States,” *Phys. Rev. Lett.* **110**, 091602 (2013) [arXiv:1212.1164 [hep-th]].
- [45] D. D. Blanco, H. Casini, L. Y. Hung and R. C. Myers, “Relative Entropy and Holography,” *JHEP* **1308**, 060 (2013) [arXiv:1305.3182 [hep-th]].
- [46] G. Wong, I. Klich, L. A. P. Zayas and D. Vaman, “Entanglement Temperature and Entanglement Entropy of Excited States,” arXiv:1305.3291 [hep-th].

- [47] M. Nozaki, T. Numasawa, A. Prudenziati and T. Takayanagi, “Dynamics of Entanglement Entropy from Einstein Equation,” arXiv:1304.7100 [hep-th].
- [48] V. Balasubramanian *et al.*, “Inhomogeneous holographic thermalization,” JHEP **1310**, 082 (2013) [arXiv:1307.7086 [hep-th]].
- [49] M. Nozaki, T. Numasawa and T. Takayanagi, “Holographic Local Quenches and Entanglement Density,” JHEP **1305**, 080 (2013) [arXiv:1302.5703 [hep-th]].
- [50] U. H. Danielsson, E. Keski-Vakkuri and M. Kruczenski, “Spherically collapsing matter in AdS, holography, and shellons,” Nucl. Phys. B **563** (1999) 279 [arXiv:hep-th/9905227].
- [51] J. Erdmenger and S. Lin, “Thermalization from gauge/gravity duality: Evolution of singularities in unequal time correlators,” JHEP **1210** (2012) 028 [arXiv:1205.6873 [hep-th]].
- [52] W. H. Baron, D. Galante and M. Schvellinger, “Dynamics of holographic thermalization,” JHEP **1303** (2013) 070 [arXiv:1212.5234 [hep-th]].
- [53] S. Kundu and J. F. Pedraza, “Spread of entanglement for small subsystems in holographic CFTs,” Phys. Rev. D **95**, 086008 (2017) [arXiv:1602.05934 [hep-th]].